ELSEVIER

Earth and Planetary Science Letters 200 (2002) 33–46

EPSL

www.elsevier.com/locate/epsl

Crystal fabric evolution in lava flows: results from numerical simulations

Gianluca Iezzi [a], Guido Ventura [b,*]

[a] *Dipartimento di Scienze della Terra, Università di Chieti, Via dei Vestini 30, I-66013 Chieti Scalo (Ch), Italy*
[b] *Osservatorio Vesuviano (Istituto Nazionale di Geofisica e Vulcanologia), Via Diocleziano 328, I-80124 Naples, Italy*

Received 8 November 2001; received in revised form 11 March 2002; accepted 18 March 2002

Abstract

The analysis of the preferred orientation of crystals (crystal fabric) in magmatic rocks has become a widely used technique for the reconstruction of the flow history. However, little is known about the evolution of the fabric during flow. Here, numerical simulations are used to study the fabric evolution of low-concentration, laminar magmatic flows (e.g. lava flows). The fabric evolution of (a) particle populations with a specified shape (cube, tablet, prism, and transitional shape) and (b) crystal populations from a lava flow is analyzed in different flow geometries (simple shear, hyperbolic and pure shear flows) assuming plane strain. Results show that fabric analysis of the whole crystal population gives little information about flow kinematics, whereas the comparative analyses of crystal sub-populations with different shapes allow us to recognize the flow geometry. Simple shear flow produces oscillating to pseudo-stable fabrics. The fabric strength is lower with respect to that of hyperbolic and pure shear flows and the preferred orientation of crystals does not coincide with the flow direction, except for large strain and specified shapes. Sub-fabrics with opposite sense of shear may also develop, depending on the crystal shape and finite strain. Pure shear and hyperbolic flows show stable to pseudo-stable fabrics. The preferred crystal orientation may or may not coincide with the flow direction according to whether flow is in pure or hyperbolic shear. Results from numerical simulations are comparable with those from experimental models and natural examples. The fabric strength depends on the number of crystals and caution must be used in extrapolating the results beyond the scale of observation. The finite strain in a sample from a lava flow from the Aeolian Islands is determined by the comparative analysis of the calculated and measured fabric parameters (fabric intensity and crystal preferred orientation). Criteria to discriminate among fabrics produced by different flow types are also provided.

Keywords: lava flows; fabric; strain; emplacement; simulation

1. Introduction

Many lava flows and dikes show a preferred orientation of crystals (crystal fabric) or elongated vesicles, or both. This feature mirrors the deformation suffered by magma during emplacement. The use of the crystal fabric as a kinematic indicator has become a widely used technique for the

* Corresponding author. Tel.: +39-81-6108329/321; Fax: +39-81-6108351.
E-mail address: ventura@ov.ingv.it (G. Ventura).

0012-821X/02/$ – see front matter
PII: S0012-821X(02)00617-9

reconstruction of flow history [1–5]. The preferred orientation of crystals is considered to give information about the local magma flow, or transport, direction. Most studies assume that: (a) crystals are biaxial particles (i.e. with a 2D shape) and (b) flowing magma deforms according to an ideal non-coaxial model [1–3,6,7]. However, crystals are solid particles with a 3D shape moving within a viscous flow that may deform according to a coaxial strain (pure shear flow), an ideal non-coaxial strain (simple shear flow) or a combination of both (hyperbolic flow) [8–10]. Previous models of the emplacement of lava flows indicate that lavas are hyperbolic flows in the near vent zone, whereas they approach simple shear near the front [9,10]. The increase of the simple shear component away from the vent is due to the gravity-driven movements of the flow [9]. In lava tubes, the central zone of the flow is characterized by a lack of a crystal preferred orientation, whereas at the top and bottom crystals show a preferred orientation consistent with the flow direction [3]. This feature indicates that a plug-type flow (i.e. a low-velocity gradient) occurs in the central zone. As the velocity gradient increases from the center to the top and bottom zones, simple shear strain also increases and crystals align to the flow direction [3]. The above observations indicate that different crystal fabrics are expected to develop in different types of flow.

Theoretical and experimental models on the behavior of particles immersed in a viscous, laminar flow ($Re \ll 10^3$) show that fabric evolution may be complex [11,12]. The development of a regularly oscillating, irregularly oscillating or stable fabric in diluted dispersions (< 1 vol%) depends on the flow type and morphological composition of the crystal population. In concentrated dispersions, fabric evolution is primarily controlled by the mechanical interaction between the particles [13].

Virtually no studies have been conducted on the fabric evolution of particle systems with shapes similar to those recognized in low-concentration magmatic flows (e.g. lavas). The only exception we know is a study on the rod-like microlites from the Little Glass Mountain, California [5]. However, these microlites are ellipsoids of revolution with aspect ratio between 10 and 20, an unusual case in most lavas of mafic to intermediate composition. In general, phenocrysts in lavas cannot be approximated to ellipsoids of revolution. They also tend to have aspect ratios less than 10 (e.g. plagioclases, pyroxenes, Fe–Ti oxides, olivines, feldspathoids) and shapes characterized by $a \neq b \neq c$, where a, b and c are the lengths of a crystal's minor, intermediate and major axes ($a \leq b \leq c$) [14,15].

The purpose of this work is to describe how crystal fabric evolves in continuous, non-fragmented, low-concentration magmatic flows, by selecting crystal shapes and flow parameters consistent with those recognized in lava flows. The paper is organized as follows: (a) a summary of the theory of particle rotation in viscous flow and a discussion of the assumptions relevant to magmatic conditions; (b) an analysis of fabric evolution in different flow types (simple shear, pure shear and hyperbolic flow) for specified particle shapes (cube, prism, tablet, intermediate shape), (c) an analysis of the crystal fabric and shape sub-fabrics of a sample from a lava flow and their evolution. The results are discussed in the light of some natural examples. A possible methodological approach to infer the finite strain from the analysis of the crystal fabric is proposed and criteria for discriminating the fabrics produced by different flow types are also supplied. The results of this study provide a tool for clarifying the kinematic significance of fabrics in low-concentration magmatic flows.

2. Theoretical background, assumptions and constraints

2.1. Theory

The equations describing the rotation of a triaxial particle immersed in a slowly moving, Newtonian viscous fluid are given in [16]. Analytical solutions of Jeffrey's equations [16] have been derived in [11,17]. Here, only the solutions are reported.

Given a coordinate system x', y', z', which is fixed in space, and a rotating coordinate system x,

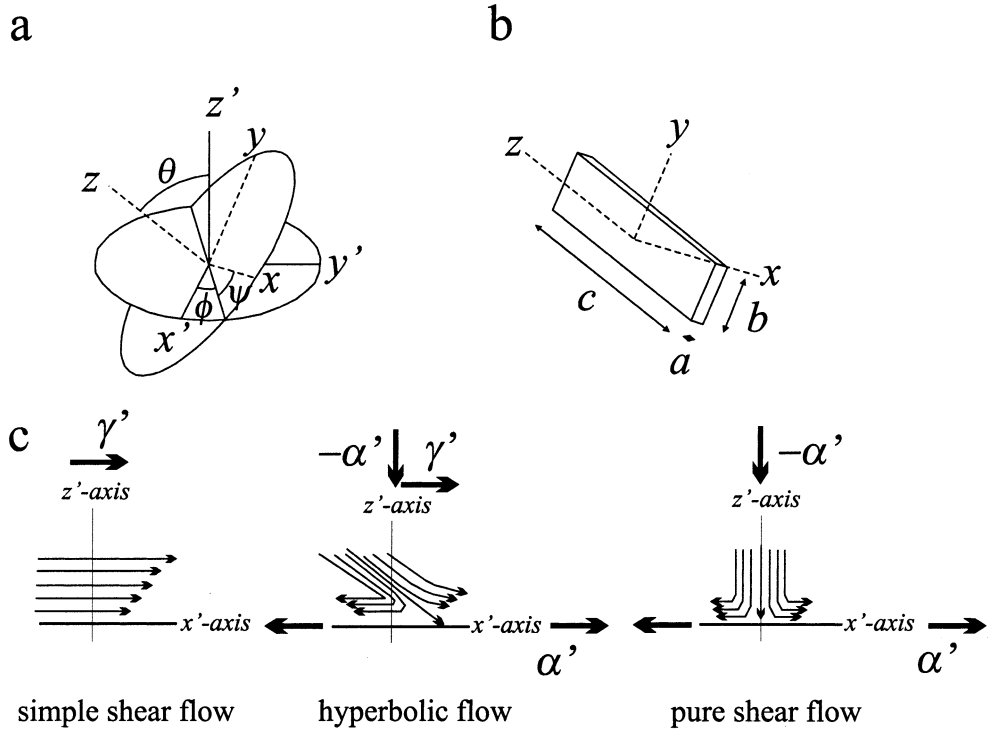

Fig. 1. (a) Euler angle definition (from [7], modified). x', y' and z' refer to the fixed axes and x, y, and z to the rotating axes. (b) Triaxial particle with axial lengths a, b and c ($a \le b \le c$). (c) Flow streamlines in simple shear, hyperbolic and pure shear flows (modified from [10]). α' and γ' are the pure shear and simple shear strain rates, respectively.

y, z, which is coherent with the axes of a rotating particle (Fig. 1a,b), the time derivative of the Euler angles (ϕ, θ, ψ), which describe the rotation of the particle, are:

$$\frac{d\phi}{dt} = (B_1\sin^2\psi - B_2\cos^2\psi)(0.5\gamma'\cos2\phi - \alpha'\sin2\phi) + (B_1 + B_2)(0.5\gamma'\sin2\phi + \alpha'\cos2\phi)\cos\theta\sin\psi\cos\psi - \gamma' \quad (1)$$

$$\frac{d\theta}{dt} = (B_1 + B_2)(0.5\gamma'\cos2\phi - \alpha'\sin2\phi)\sin\theta\sin\psi\cos\phi + (B_1\cos^2\psi B_2\sin^2\psi)(0.5\gamma'\sin2\phi + \alpha'\cos2\phi)\sin\phi\cos\phi \quad (2)$$

$$\frac{d\psi}{dt} = B_3(0.5\gamma'\sin2\phi + 2\alpha'\cos2\phi)(1 + \cos^2\theta)\sin\psi\cos\psi - B_3\alpha'\sin2\phi\cos\theta(\cos^2\psi - \sin^2\psi) - 0.5\gamma'\cos\theta - \frac{d\phi}{dt}\cos\theta \quad (3)$$

where α' and γ' are the pure shear rate and simple shear rate, respectively. B_1, B_2 and B_3 are particle shape parameters:

$$B_1 = (b^2 - c^2)/(b^2 + c^2) \quad (4)$$

$$B_2 = (c^2 - a^2)/(c^2 + a^2) \quad (5)$$

$$B_3 = (a^2 - b^2)/(a^2 + b^2) \quad (6)$$

where a, b and c are the lengths of the particle axes ($a \le b \le c$) (Fig. 1b).

Assuming plane strain, at a large distance from the particle, the undisturbed flow is specified by the velocity gradient tensor V [11,17]:

$$V = \begin{bmatrix} \alpha' 0 \\ 00 \\ 00 \end{bmatrix} \quad (7)$$

Hyperbolic flows are characterized by $\alpha' \neq 0$ and $\gamma' \neq 0$, simple shear flows by $\alpha' = 0$ and $\gamma' \neq 0$, and pure shear flows by $\alpha' \neq 0$ and $\gamma' = 0$ [9,10] (Fig. 1c).

Eqs. 1–7 indicate that the position of a rotating triaxial particle with respect to the fixed coordinate system is determined from: (a) the shape, (b) the initial position and (c) the flow geometry. If these parameters are defined, it is possible to analyze the fabric evolution of a multiparticle system by assigning an initial position to each particle and by incrementing the finite strain [γ (simple shear), α (pure shear) or a combination of the two] at a constant strain rate. In this work, the fabric evolution of multiparticle systems is analyzed using the *Muple* software [18]. The basic features and routines of *Muple* may be found in the original paper [18] and a summary is reported in Appendix 1.

2.2. Assumptions and physical constraints

The above equations are applicable to magmatic flows only if particular physical conditions are satisfied. These include:

1. particles do not interact each other [13];
2. particles do not deform;
3. lack of variation in particle shape (e.g. due to growth) during the flow;
4. continuous (non-fragmented) laminar flow (liquid plus particles) ($Re \ll 10^3$);
5. Newtonian flow behavior and constant strain rate.

Condition (1) may not be satisfied by all magmatic flows, but should hold for dilute flows such as sub-aphyric basalts and rhyolites (e.g. obsidians). According to [5], dilute dispersions are characterized by $nl^3 \ll 1$, where n is the number density (number of crystals/m^3) and l is the length. This is the condition for which no interaction between particles occurs in the flow. Condition (2) is generally satisfied in all non-fragmented flows for which crystals are rigid, whereas the viscous melt has a Newtonian or a Bingham behavior [19]. Condition (3) is generally not satisfied: the shape of crystals reflects the growth rate, which strongly depends on the cooling rate and fluid content of the magma [20,21]. However, if the cooling rate and fluid content are constant, it may reasonably be assumed that the shape (i.e. the axial ratio) does not change during the growth. Condition (4) is valid for the majority of lava flows [22], although rare examples have been cited for high-velocity, partly turbulent flows [23]. Condition (5) is not always satisfied. Flowing magmas generally show a Bingham behavior [24,25] and a variable strain rate during emplacement. However, [7] reports that Jeffrey's analysis is generally valid for non-Newtonian media (e.g. pseudoplastic and elastoviscous flows) and, according to [26], the strain rate may be considered to be constant in near-vent flows (i.e. distances from the vent in the order of $\sim 10^1$–10^2 m). In the following, we assume that the strain rate remains constant, at least at a length scale of 10^{-1}–10^{-3} m, which is the scale of practical observation (thin section). Strain rate may vary within the flow at a larger scale, however, we limit our analysis to a 10^{-1}–10^{-3} m length scale. Finally, the flow must be avesicular, since vesicles induce an internal deformation that may locally modify the bulk flow geometry [27] and, as a consequence, the crystal fabric.

3. Fabric evolution of particle systems of the same shape

3.1. Particle shape and fabric parameters

Taking into account the practical scale of observation (10^{-1}–10^{-3} m) and the shape of crystals generally occurring in lava flows [14,15], we have selected four crystal-shape populations for detailed study (Fig. 2). Each population consists of

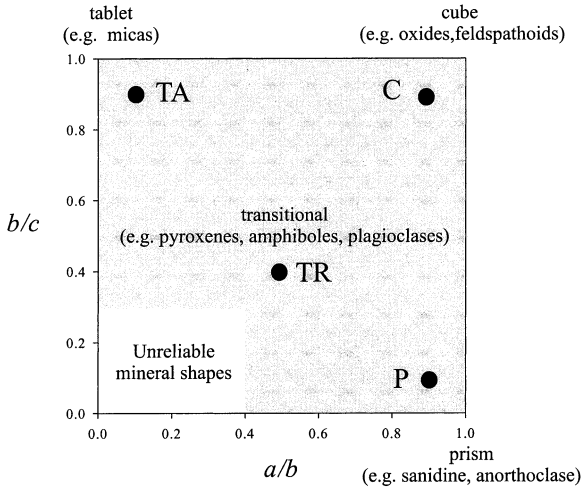

Fig. 2. Mineral shape in terms of the three axial lengths a, b, c (modified from [14]). The crystal shapes selected for the fabric analysis are shown as dots. C (cube), P (prism), TA (tablet) and TR (transitional) are the abbreviations used in the text.

112 particles. Population C is characterized by pseudo-cubic particles ($a/b = b/c = 0.9$), population P contains prismatic particles ($a/b = 0.9$; $b/c = 0.1$), population TA consists of tablet-like particles ($a/b = 0.1$; $b/c = 0.9$) and population TR is characterized by particles with a shape transitional among the previous ones ($a/b = 0.5$; $b/c = 0.4$). We analyze the fabric evolution of each population in three flow types: simple shear flow, pure shear flow and hyperbolic flow (Fig. 1c). Lava flows are characterized by strain rates in the range 10^{-1}–10^{-5} s^{-1} [28]. Finite strains calculated from the preferred orientation of crystals in obsidians and andesites generally do not exceed $\gamma \simeq 10$ [3,5]. In the numerical simulations (Eqs. 1–3 and 7) we select the following strain rates:

1. $\alpha' = 0$ and $\gamma' = 5 \times 10^{-2}$ s^{-1} for the simple shear flow;
2. $\alpha' = \gamma' = 5 \times 10^{-2}$ s^{-1} for the hyperbolic flow;
3. $\alpha' = 5 \times 10^{-2}$ s^{-1} and $\gamma' = 0$ for the pure shear flow.

We perform the calculation from α or $\gamma = 0$ up to α or $\gamma = 50$. Each population is assumed initially (zero strain) to be isotropic, without a preferred orientation.

The fabric evolution is defined by two parameters:

1. The fabric intensity $I = 7.5\ \Sigma_{i=1}^{3}\ (E_i - 1/3)$, where E_i are the normalized eigenvalues of the orientation tensor [29]. This parameter is a measure of fabric strength, i.e. of fabric anisotropy. $I = 0$ indicates an isotropic fabric. As the number of aligned particles increases, I also increases.
2. The angle δ between the eigenvector associated with the largest eigenvalue of the orientation tensor and the flow direction (the x'-axis) in a x'–z' plane. δ is independent of the number of aligned particles. This angle represents the preferred orientation of the particles with respect to the flow direction. The structural significance of the fabric parameters I and δ is illustrated in Fig. 3a. The reference frame adopted in this study is shown in Fig. 3b. For reasons of symmetry, the angle is referred to the first and fourth quadrants. In a sinistral simple shear, rotation of the preferred fabric orientations from negative to positive δ values is consistent with the shear sense whereas rotations from positive to negative δ values indicate backward rotations, opposite to the imposed sense of shear.

In this paper, the variations of I and δ with respect to γ and α are analyzed. Consequently, the results of the numerical simulation do not change

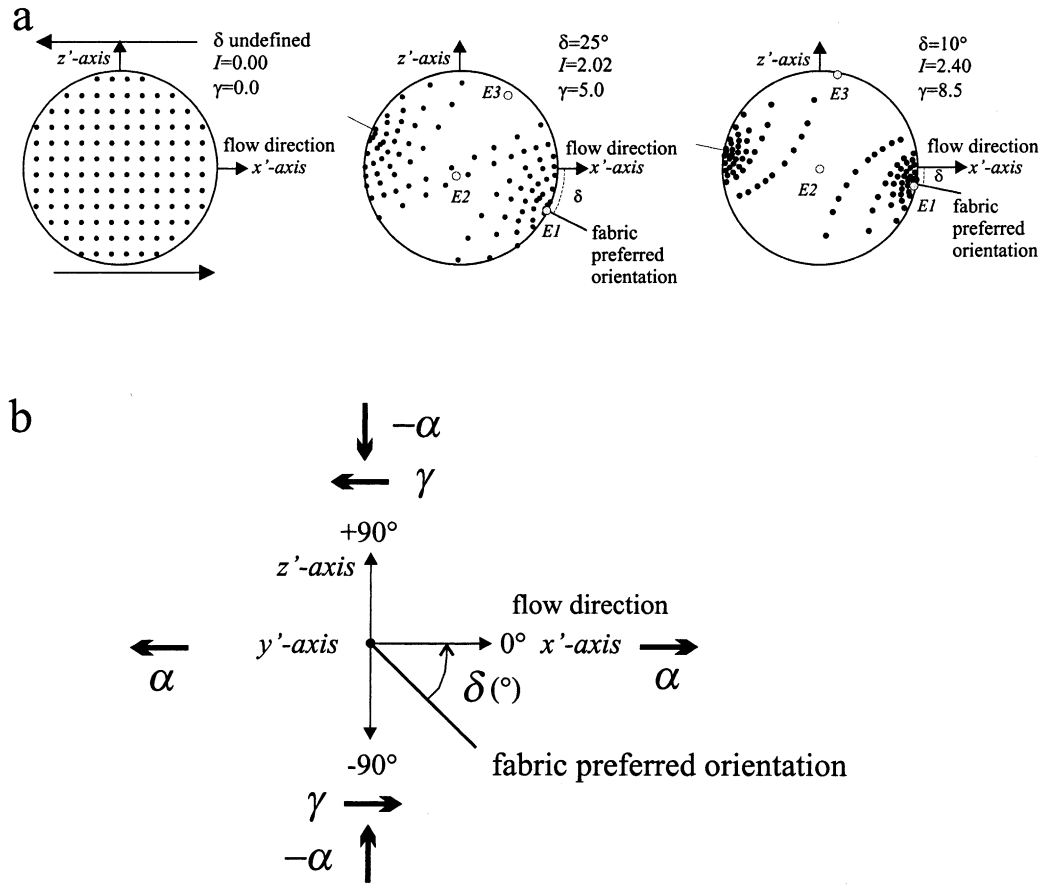

Fig. 3. (a) Model of fabric evolution in a multiparticle system of 120 rigid inclusions with axial ratio 1:1:4 in a sinistral simple shear flow. Black dots represent the long axes of the particles (equal angle, lower hemisphere projection on a x'–z' plane). Gray, larger dots represent the orientation of the eigenvectors associated to the eigenvalues E_1, E_2, and E_3 of the orientation tensor. The finite strain γ increases from left to right. The values of the fabric parameters I, δ and γ are also reported. (b) Geometry adopted for the analysis of crystal preferred orientation. A sinistral simple shear γ is imposed. The pure shear α parallels the x'-axis and z'-axis.

if the strain rate (γ' or α') varies because I and δ depend on the finite strain (αor γ) [29] and not on the strain rate. The fabric evolution of the four selected populations in the different flow types is shown in Fig. 4.

3.2. *Fabric evolution in simple shear, hyperbolic and pure shear flows*

In a simple shear flow (Fig. 4), the fabric of population C is oscillatory with periodic variations. The maximum I value is 0.1. The fabric intensity of population P increases irregularly up to $I=4$ at $\gamma=33$ and then slightly decreases ($I=3.2$ at $\gamma=50$). Population TR shows a more complex, irregular oscillating fabric. The maximum I is 2 at $\gamma=14$ and the minimum I is 0.3 at $\gamma=28$. Population TA is characterized by an initial increase of I ($I=1$ at $\gamma=15$) and by a slightly oscillating pattern with I values between 0.9 and 1.1 at $15\geq\gamma\geq50$. Populations TA and P show a preferred orientation approaching that of the x'-axis only at large strains ($\gamma\geq28$). Population C never attains a stable preferred orientation showing pseudo-periodic δ variations. Population TR is characterized by significant δ variations. This population reaches a stable preferred orientation, which is that of the x'-axis, at $\gamma\geq40$. As

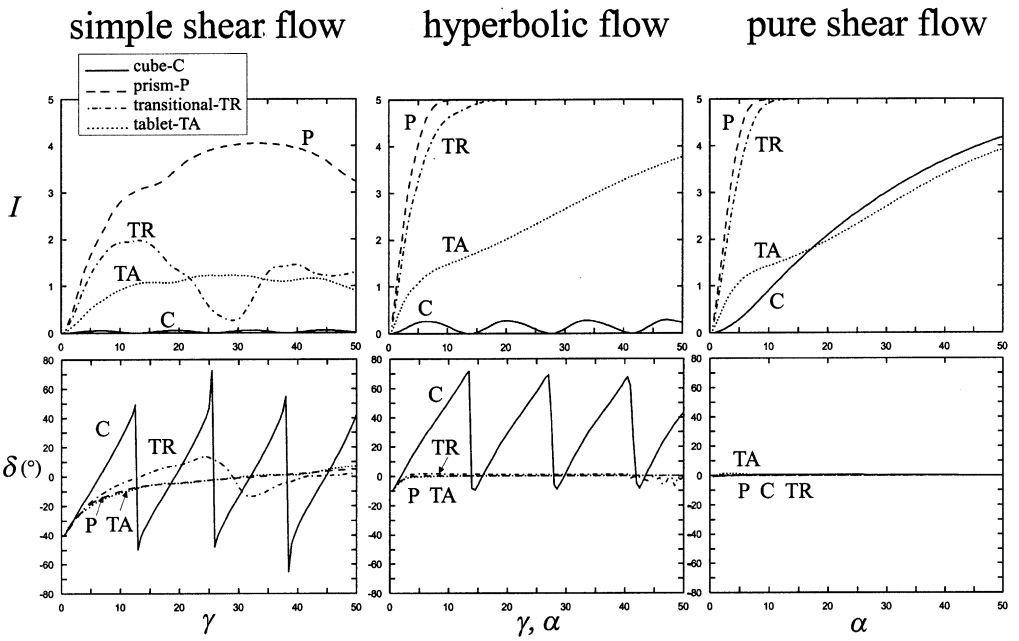

Fig. 4. Results of numerical simulations for cube, prism, tablet, and transitional shapes in simple shear, hyperbolic and pure shear flows. I is the fabric intensity. δ is defined in Fig. 3. Populations consist of 112 particles. At $\gamma=0$ and $\alpha=0$, $I=0$. At $I=0$, δ is undefined. On γ or α vs. δ plots, δ is reported for $I>0$.

strain increases, populations C and TR are characterized by negative to positive δ variations and, on the opposite, by positive to negative δ variations. These latter variations indicate backward rotation of the particles (i.e. sense of rotation opposite to the imposed sense of shear). Population TR shows a backward rotation at $25 \leq \gamma \leq 33$.

In a hyperbolic flow (Fig. 4), the fabric intensity of the populations P, TR and TA increases progressively up to $I=5$ as the strain increases. However, the rate at which the fabric strength of populations P and TR increases is higher with respect to that of population TA. Population C shows a periodic fabric variation with a maximum I value of 0.3. The populations P, TR and TA show a stable fabric preferred orientation at $\gamma=\alpha \geq 10$. The fabric preferred orientation is consistent with the flow direction. Population C shows periodic δ variations with values ranging from -10 to 70.

In a pure shear flow (Fig. 4), all populations show a progressive increase of I. The rate of I increase is higher for populations P and TR. In all populations, fabric preferred orientation corresponds to the flow direction: $\delta \simeq 0°$ at α between 1 and 50.

The fabric evolutions shown in Fig. 4 have been obtained using populations of 112 particles. In Fig. 5, the fabric evolution of two populations with particles of the same shape (transitional) but with a different number of particles (32 and 112) is shown. No significant differences in both I and δ occur between the two populations in hyperbolic and pure shear flows. Some divergence between the two populations may be recognized in simple shear flow, mainly for $\gamma>20$. However, the general pattern of the fabric evolution parameters is similar. Using cubes, prisms or tablets (not shown), the intensity increases as the number of particles in each population decreases.

4. Fabric evolution of particle systems of different shape: an example from a lava flow

4.1. Crystal shapes and fabric parameters

We here analyze the fabric evolution of a sys-

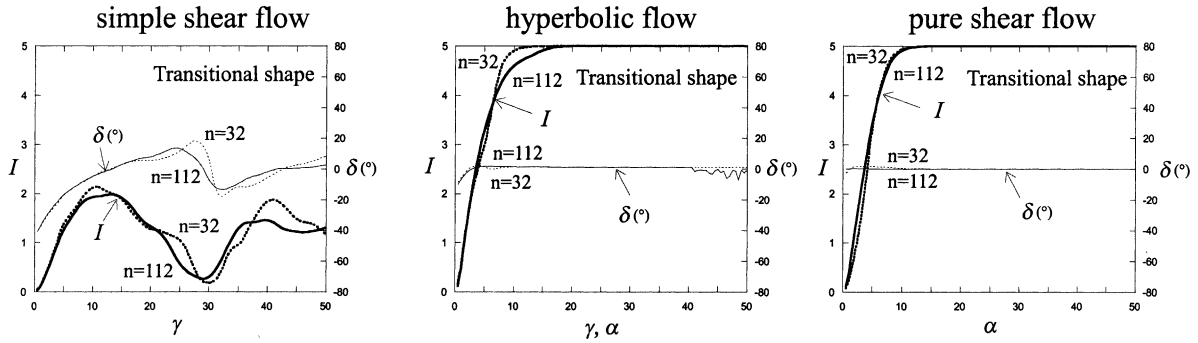

Fig. 5. Results of the numerical simulation for a transitional shape in a simple shear, hyperbolic and pure shear flow using populations of different number (n) of particles. I is the fabric intensity. δ is defined in Fig. 3. At $\gamma=0$ and $\alpha=0$, $I=0$. At $I=0$, δ is undefined. On γ or α vs. δ plots, δ is reported for $I>0$.

tem consisting of particles with different shape and propose a possible methodological approach to the analysis of the crystal fabric of lava flows. We select shapes from a sample collected in the central portion of basaltic lava flow from the Mount Fossa delle Felci volcano (Salina Island, Aeolian Islands, Italy; Fig. 6a). The collected sample is oriented (Fig. 6a). The x-axis is parallel to the flow direction and the z-axis is orthogonal to the substratum on which the flow moved. Crystal shapes have been collected from three thin sections. The sections are parallel to the x–y, x–z and y–z planes (Fig. 6a). The rock shows a sub-aphyric texture and consists of an assemblage of crystals (plagioclase, clinopyroxene, olivine) immersed in a glassy matrix with Fe–Ti oxides.

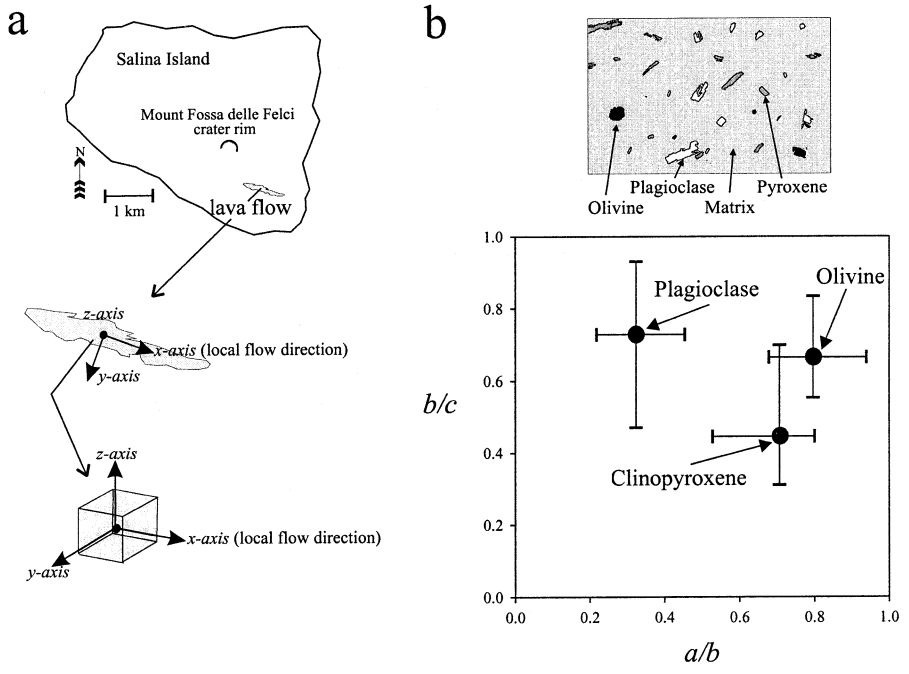

Fig. 6. (a) Location map of the Mount Fossa delle Felci lava flow and orientation of the sample and of the three orthogonal thin sections. (b) Shape of plagioclase, pyroxene and olivine in the lava flow from Mount Fossa delle Felci. Bars indicate the variation in measurements and dots the arithmetic mean.

The crystals have a number density $n = 7.6 \times 10^{10}$ m^{-3} and a mean length $l = 8.7 \times 10^{-4}$ m; nl^3 is 0.5 and the volume fraction of crystals is 0.017. These values indicate that the lava flow was a low-concentration suspension. The abundance of Fe–Ti oxides is about 0.02 vol%. The relative abundance of the phenocrysts and their number in a thin section is: plagioclase = 57% ($n = 113$), clinopyroxene = 26% ($n = 52$) and olivine = 16% ($n = 31$). Neglecting the Fe–Ti oxides, the shape of the main phases has been determined following [2,14,15].

The results are summarized in Fig. 6b, where the arithmetic mean and the variation range of the axial ratios (a/b and b/c) of the mineral phases are shown. The parameters I and δ have been also calculated. Plagioclases are characterized by $a/b = 0.33$, $b/c = 0.75$, $I = 0.9$ and $\delta = -6°$, clinopyroxenes by $a/b = 0.7$, $b/c = 0.45$, $I = 1.4$ and $\delta = 5°$, olivines by $a/b = 0.8$, $b/c = 0.71$ and $I = 0.3$ and $\delta = 18°$. For the whole population, I and δ are 0.9 and $-5°$, respectively.

Taking into account the particle number and the mean axial ratios of the three main phases, we consider a population of 196 particles (crystals) as representative of the sample. This population consists of three sub-populations: 113 plagioclases, 52 clinopyroxenes and 31 olivines. We analyze the fabric evolution of each sub-population and of the whole crystal population in simple shear, hyperbolic and pure shear flows. The flow parameters are the same as used in Section 3 and the fabric is assumed to have been isotropic at zero strain.

4.2. Evolution of the crystal fabric in simple shear, hyperbolic and pure shear flows

Results of the analysis are shown in Fig. 7. In a simple shear flow, both the mineral sub-populations and the whole population show an irregular oscillating fabric. I values do not exceed 1.7. The preferred orientation is also oscillating with the larger variations (up to 140°) in the olivine sub-

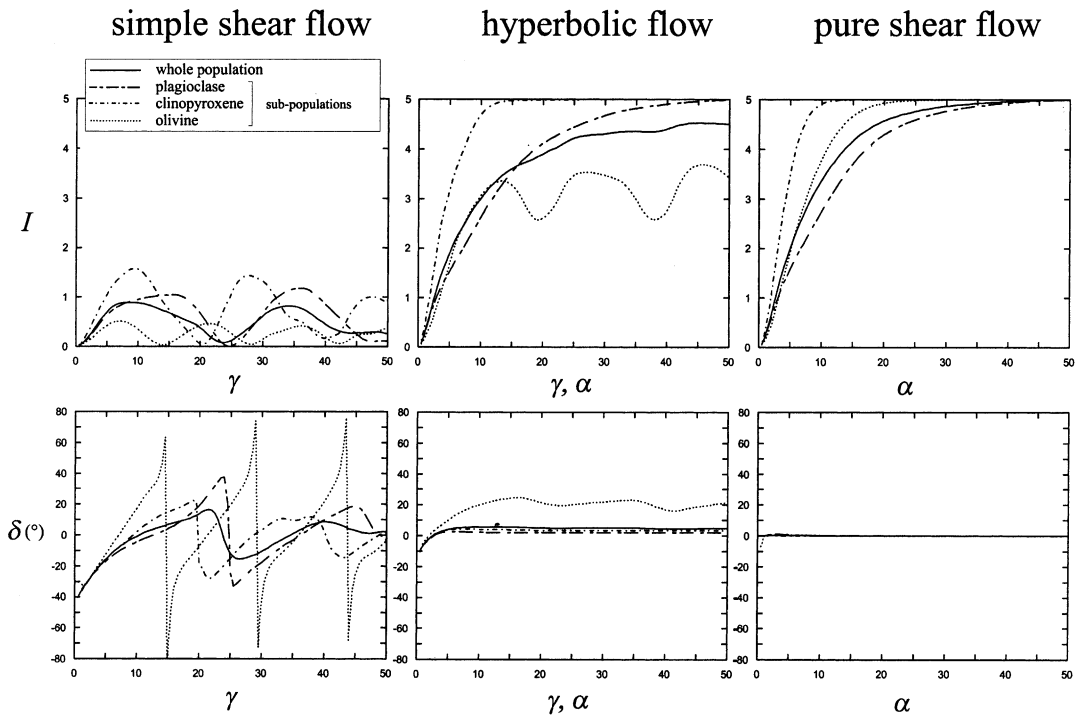

Fig. 7. Results of the numerical simulation for plagioclase, clinopyroxene, olivine (Fig. 6) and whole rock population from a lava flow of Mount Fossa delle Felci volcano in a simple shear, hyperbolic and pure shear flow. I is the fabric intensity. δ is defined in Fig. 3. At $\gamma = 0$ and $\alpha = 0$, $I = 0$. At $I = 0$, δ is undefined. On γ or α vs. δ plots, δ is reported for $I > 0$.

population. None of the sub-populations reaches a stable orientation. Backward rotation occurs in both plagioclase and clinopyroxene sub-populations as well as in the whole population for $20 \leq \gamma \leq 26$ and $\gamma \geq 40$.

In a hyperbolic flow, the fabric strength of the plagioclase and clinopyroxene sub-populations, as well as of the whole population, increases progressively as strain increases. However, the rate at which I increases is largest for the clinopyroxenes ($I = 5$ at $\alpha = \gamma = 26$). The plagioclase sub-population reaches the maximum intensity ($I = 5$) at $\alpha = \gamma = 48$. The maximum fabric strength of the whole population is 4.6 at $\alpha = \gamma = 46$. The fabric strength of the olivine sub-population regularly increases up to $\alpha = \gamma = 13$. At higher strain, I shows an irregularly oscillating pattern with values between 2.6 and 3.7. The preferred orientation of the plagioclase and clinopyroxene sub-populations and of the whole populations reaches a stable value at $\alpha = \gamma \geq 10$. However, the angle between the x'-axis and the fabric preferred orientation is 3° for the plagioclases, 5° for the clinopyroxenes and 8° for the whole population. Olivine sub-population shows an irregularly oscillating δ pattern ($16° \leq \delta \leq 25°$) at $\alpha = \gamma \geq 16$.

In a pure shear flow, the fabric strength of all the sub-populations and of the whole population increases progressively up to $I = 5$. The rate of the fabric intensity increase of the clinopyroxene sub-population is larger than that of the olivine sub-population, whole population and plagioclase sub-population, respectively. The preferred orientation of all the sub-populations and of the whole population is that of the x'-axis at $\alpha \geq 3$.

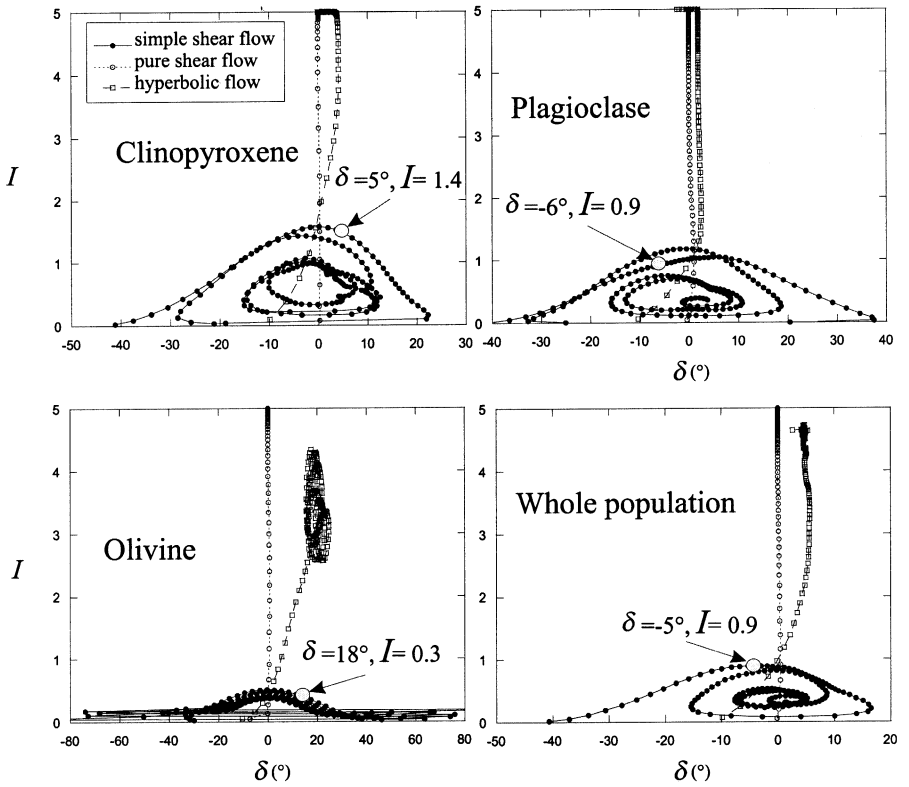

Fig. 8. δ vs. I curves from the results of the numerical models shown in Fig. 7. Full dots (simple shear flow), empty dots (pure shear flow) and squares (hyperbolic flow) are increments of finite strain ($\Delta\gamma$ or $\Delta\alpha = 1$). The fabric parameters I and δ determined in a sample from a lava flow of Fossa delle Felci volcano are reported as gray dots.

4.3. Determination of the finite strain from fabric analysis

In Fig. 8, the I and δ values determined for each crystal sub-population are reported on theoretical δ vs. I curves. The δ values are positive in the clinopyroxene and olivine sub-populations whereas they are negative in the plagioclase sub-population and in the whole population. The fabric parameters of both the sub-populations and whole population lie on the curves of simple shear flow (Fig. 8). This feature also suggests that if particle interaction occurred it must have played a minor role in the fabric evolution. The determined I and δ values of each sub-population may be used to infer the finite simple shear strain graphically (Fig. 8). The clinopyroxene parameters indicate $\gamma = 11$, while the plagioclase and olivine parameters indicate $\gamma = 9$ and $\gamma = 10$, respectively. The parameters of the whole rock are consistent with $\gamma = 8$. As a result, the calculated values of the finite strain γ are between 8 and 11. This estimate has significance only for the analyzed rock volume and cannot be representative of the whole lava flow. However, the calculated γ values are comparable with previous estimates on samples from other lava flows (i.e. obsidians from Little Glass [5] and andesites from Porri volcano [3]), which also underwent simple shear deformation with values of finite strain $\gamma \approx 10$.

5. Discussion

The results of this study allow us to put some constraints on the evolution of crystal fabric in low-concentration magmatic flows. According to Eqs. 1–7, the fabric is determined by: (a) the relative abundance of crystal populations with different shape, (b) the flow type (simple shear, hyperbolic, pure shear flow), and (c) the strain magnitude.

In populations characterized by a different number of crystals of the same shape, the fabric parameters (I and δ) do not differ significantly in hyperbolic and pure shear flows (Fig. 5). In simple shear flows, however, some differences between the values of the fabric parameters have been observed. As a consequence, the number density n must be taken into account when analyzing crystal fabrics and caution must be used in extrapolating the fabric parameters from the sample scale (e.g. thin section; length scale 10^{-1}–10^{-3} m), where n is generally constant, to a larger scale (e.g. the bulk flow), where n may vary. We conclude that the method proposed here for the calculation of finite strain from fabric analysis (Fig. 8) may be useful to determine the strain pattern of a lava flow when (a) a large set of samples is available and (b) samples have similar n values.

The results from numerical simulation show that in systems containing crystal populations of different shape, irregular to periodic oscillations of the fabric parameters characterize simple shear flows whereas a stable fabric characterizes pure shear flow (Figs. 4 and 7). This observation is consistent with the results of experimental models on 2D particles immersed in a viscous flow ([30] and references therein) and theoretical models on rod-like particles [5]. Depending on the crystal shape and on the ratio between simple shear (non-coaxial) and pure shear (coaxial) strain, the fabric may evolve cyclically or to a stable orientation.

Simple shear flows always show lower fabric strength with respect to hyperbolic flows and to pure shear flows. A low fabric anisotropy in a lava flow or dike is generally interpreted to be indicative of a plug-type flow (e.g. [3,31]) or turbulent movements [32]. However, the low anisotropy may be due to a pure shear flow at the early stages or a simple shear flow. This conclusion is supported by results from recent experimental studies on the anisotropy of magnetic susceptibility in lava flows [33]. These studies show that lavas subjected to shearing yield a lower degree of anisotropy even when high strains are imposed on it.

In a simple shear flow (Fig. 4), semi-periodic oscillations characterize particles with $a \neq b \neq c$ (transitional shape) whereas periodic oscillations characterize particles with $a \simeq b \simeq c$ (cubic shape). Pseudo-stable fabrics characterize particles with $a \simeq b \ll c$ (prism) or $a \ll b \simeq c$ (tablet) at $\gamma \geq 28$. However, the preferred orientation of prisms and tablets mirrors that of the flow direction

only at large strain ($\gamma \geq 40$). Prisms and tablets are therefore good indicators of the flow direction only in simple shear flows that suffered high deformation. On the contrary, the preferred orientation of prism, tablet, cube and transitional shapes in a pure shear flow is always indicative of the (local) flow direction. These observations suggest that the crystals preferred orientation is not representative of the flow direction for lava flows that: (a) move in simple shear [5,10] and (b) are characterized by low values of finite strain [3,5].

In a simple shear flow, the fabric evolution of the crystal sub-populations and whole population of a sample from a basaltic lava flow from Mount Fossa delle Felci on Salina (Figs. 6–8) is characterized by irregular oscillations with backward rotations of crystals. None of the populations reaches a stable orientation. The numerical analyses on particles of different shape (e.g. cubes and transitional shapes in Fig. 4) also indicate that backwards rotation of crystals may occur in both simple shear and hyperbolic flows. Consequently, populations with low fabric strengths and preferred orientations indicative of opposite shear sense may be interpreted as products of a simple shear flow or a hyperbolic flow. Accordingly, the fabric analysis of the whole crystal population gives little information about the (local) flow type, flow direction and strain magnitude, whereas the comparative analysis of the crystal sub-populations may be a better guide to infer the flow type and the finite strain.

The results of the analysis presented here allow us to explain the features of the fabric of some lava flows. Ventura et al. [3] report the occurrence of a crystal fabric characterized by the lack of a preferred orientation in the central portion of a andesitic lava flow from the southern flank of the Porri volcano (Aeolian Islands, Southern Italy). Samples from the top and base of the flow show a higher strength. The preferred orientation of these samples approaches that of the flow direction moving from the center to the top and bottom of the flow. The fabric of the central portion of the flow has been interpreted to result from a plug-type flow; the fabric from the top and base of the flow has been interpreted to result from a simple shear flow. The results from numerical simulations are consistent with this interpretation: the central zone of the flow is characterized by low strain whereas the upper and basal zones are affected by higher strain. Moving from the center to the top and basal zones, the strain increases according to a simple shear or hyperbolic flow. This interpretation is supported by results from numerical models on strain variations in lava tubes [34].

Higgins [14] has described the preferred orientations of crystals at different heights above the base of an andesitic lava flow from Mt. Taranaki (New Zealand). Samples at the base of the lava flow show a well-defined absolute maximum in the crystal preferred orientation, which is parallel to the flow direction (fig. 11 in [14]). Samples from the top of the flow show an absolute maximum, which is not parallel to the flow direction, and second-order relative maxima. In the light of the results from the present study, two different deformation patterns may be proposed: (a) pure shear occurs at the bottom and simple shear, or a combination of simple and pure shear, at the top; (b) simple shear strain, or the simple shear component in a hyperbolic flow, increases from the top to the bottom of the flow. Deformation pattern (a) disagrees with results from experimental models on the strain pattern in lava flows with an upper free surface [9]. These models show that lava flows are characterized by a nearly constant component of pure shear and by a component of simple shear that increases from the top to the bottom. Consequently, we conclude that the fabric features of the Mt. Taranaki lava flow mirror the deformation pattern depicted in (b).

All the results from this study indicate that: (a) the kinematics and deformation pattern of low-concentration magmatic flows can be analytically reconstructed using crystal shapes and (b) field data may be compared with results from numerical models if measurements of the crystal preferred orientation and fabric intensity are available. Further studies will focus on the analysis of the fabric evolution in flows with time-variable flow geometry.

6. Conclusions

The results of this study may be summarized in four points:

1. The crystal fabric of a lava flow depends on: (a) the relative amount of crystal populations with different shape, (b) the flow type (simple shear, hyperbolic, pure shear flow), and (c) the strain magnitude.
2. The fabric analysis of the whole crystal population of a lava flow gives little information about flow kinematics, whereas the comparative analysis of crystal (shape) sub-populations may provide a good tool for inferring the flow type. The fabric parameters of different sub-populations may be used to determine the finite strain.
3. Unstable crystal fabrics characterize lavas moving in simple shear. The crystal shape sub-fabrics and the whole rock fabric are characterized by low fabric strength and by a crystal preferred orientation that does not coincide with that of the flow direction. Crystal shape sub-fabrics with opposite senses of shear may also develop.
4. Stable crystal fabrics characterize lavas moving in pure shear. The crystal shape sub-fabrics and the whole rock fabric are characterized by high fabric strength and by a crystal preferred orientation that coincides with the flow direction. Depending on the shape of crystals, hyperbolic flows show stable to pseudo-stable fabrics. The preferred crystal orientations may or may not coincide with flow direction.

Acknowledgements

We thank Josef Jezek for providing us the *Muple* software and Michael Manga for a helpful review of the manuscript. We would like to thank Giuseppe Vilardo for fruitful discussions. The perceptive reviews of Jon Castro, Olivier Merle and Chris Kilburn greatly improved the manuscript. Also, we would like to thank Anny Cazenave for the editorial handling.*[AC]*

Appendix 1

To solve Eqs. 1–3, *Muple* program requires the following input parameters: (a) the number of particle populations with a fixed axial ratio, (b) the length of the particle axes (*a, b, c*) of each population, (c) the number of particles in each population, (d) the components γ' and α' of the velocity gradient tensor V (Eq. 7), (e) the time step Δt used for the calculations. As $\gamma' = \gamma/t$ ($\alpha' = \alpha/t$) is constant, $\gamma(\alpha)$ increases as t increases. For solving Eqs. 1–3, a subroutine of IMSL that performs the fourth- and fifth-order Runge–Kutta method is found to be satisfactorily precise with respect to the considered number of time increments [18]. The provided output are: t, I and δ; t is used to estimate γ (α) at each time step through the relationship $\gamma = \gamma' t$ ($\alpha = \alpha' t$).

References

[1] D. Shelley, Determining paleo-flow directions from groundmass fabrics in the Lyttelton radial dykes, New Zealand, J. Volcanol. Geotherm. Res. 25 (1985) 69–79.
[2] Y. Wada, Magma flow directions inferred from preferred orientations of phenocrysts in a composite feeder dyke, Miyake-Jima, Japan, J. Volcanol. Geotherm. Res. 49 (1992) 119–126.
[3] G. Ventura, R. De Rosa, E. Colletta, R. Mazzuoli, Deformation patterns in high- viscous lava flows inferred from the preferred orientation and tiling of crystals. An example from Salina (Aeolian Islands, Southern Tyrrhenian Sea – Italy), Bull. Volcanol. 57 (1996) 555–562.
[4] J.V. Smith, Interpretation of domainal groundmass textures in basalt lavas of the southern Lamington Volcanics, eastern Australia, J. Geophys. Res. 103 (B11) (1998) 27383–27391.
[5] M. Manga, Orientation distribution of microlites in obsidian, J. Volcanol. Geotherm. Res. 86 (1998) 107–115.
[6] L.J. Reed, E. Tryggvason, Preferred orientations of rigid particles in a viscous matrix deformed by pure shear and simple shear, Tectonophysics 24 (1974) 85–98.
[7] C. Ferguson, Rotations of elongate rigid particles in slow non-newtonian flows, Tectonophysics 60 (1979) 247–262.
[8] J.V. Smith, S. Yamauchi, Y. Miyake, Microshear zones in a Miocene submarine dacite dome of southwest Japan, Bull. Volcanol. 55 (1993) 438–442.
[9] O. Merle, Internal strain within lava flows from analogue modelling, J. Volcanol. Geotherm. Res. 81 (1998) 189–206.
[10] G. Ventura, The strain path and emplacement mechanism of lava flows: an example from Salina (Southern Tyrrhe-

nian Sea, Italy), Earth Planet. Sci. Lett. 188 (2001) 229–240.
[11] J. Jezek, R. Melka, K. Schulamnn, Z. Venera, The behaviour of rigid triaxial particles in viscous flows-modeling of fabric evolution in a multiparticle system, Tectonophysics 229 (1994) 165–180.
[12] A.L. Yarin, O. Gottleib, I.V. Raisman, Chaotic rotation of triaxial ellipsoids in simple shear flow, J. Fluid Mech. 340 (1997) 83–100.
[13] B. Ildefonse, D. Sokoutis, N.S. Manktelow, Mechanical interactions between rigid particles in a deforming ductile matrix. Analogue experiments in simple shear flow, J. Struct. Geol. 10 (1992) 1253–1266.
[14] M.D. Higgins, Crystal size distributions and other quantitative textural measurements in lavas and tuff from Egmont volcano (Mt. Taranaki), New Zealand, Bull. Volcanol. 58 (1996) 194–204.
[15] M.D. Higgins, Measurement of crystal size distribution, Am. Miner. 85 (2000) 1105–1116.
[16] G.B. Jeffery, The motion of elipsoidal particles immersed in a viscous fluid., Proc. R. Soc. London A102 (1922) 161–179.
[17] B. Freeman, The motion of rigid ellipsoidal particles in slow flow, Tectonophysics 113 (1985) 163–183.
[18] J. Jezek, Software for modeling the motion of rigid triaxial ellipsoidal particles in viscous flow, Comp. Geosci. 20 (3) (1994) 409–424.
[19] F.J. Spera, A. Borgia, J. Strimple, Rheology of melts and magmatic suspensions: design and calibration of concentric cylinder viscometer with application to rhyolitic magma, J. Geophys. Res. 93 (B9) (1988) 10273–10294.
[20] K.V. Cashman, Relationship between plagioclase crystallization and cooling rate in basaltic melts, Contrib. Mineral. Petrol. 113 (1993) 126–142.
[21] A.G. Simakin, P. Armienti, M.B. Epel'baum, Coupled degassing and crystallization: experimental study at continuous pressure drop, with application to volcanic bombs, Bull. Volcanol. 61 (1999) 275–287.
[22] M. Dragoni, Modelling the reology and cooling of lava flows. In: C. Kilburn, G. Luongo G. (Eds.), Active Lavas, UCL Press, 1993, pp. 235–261.
[23] S. Baloga, P.D. Spudis, J.E. Guest, The dynamics of rapidly emplaced terrestrial lava flows and implications for planetary volcanism, J. Geophys. Res. 100 (B12) (1995) 24509–24519.
[24] H. Pinkerton, R.J. Stevenson, Methods of determining the rheological properties of magmas at sub-liquidus temperatures, J. Volcanol. Geotherm. Res. 53 (1992) 47–66.
[25] M.O. Saar, M. Manga, K.V. Cashman, S. Fremouw, Numerical models of the onset of yield strength in crystal-melt suspensions, Earth Planet. Sci. Lett. 187 (2001) 367–379.
[26] A. Tallarico, M. Dragoni, Viscous newtonian laminar flow in a rectangular channel: application to Etna lava flow, Bull. Volcanol. 61 (1999) 40–47.
[27] D.J. Stein, F. Spera, Rheology and microstructure of magmatic emulsions: theory and experiments, J. Volcanol. Geotherm. Res. 49 (1992) 157–174.
[28] H. Pinkerton, G. Norton, Rheological properties of basaltic lavas at sub-liquidus temperatures: laboratory and field measurements on lavas from Mount Etna, J. Volcanol. Geotherm. Res. 68 (1995) 307–323.
[29] R.J. Lisle, The use of the orientation tensor for the description and statistical testing of fabrics, J. Struct. Geol. 7 (1985) 115–117.
[30] A. Nicolas, Kinematics in magmatic rocks with special reference to gabbros, J. Petrol. 33 (4) (1992) 891–915.
[31] E. Canon-Tapia, G.P.L. Walker, E. Herrero-Bervera, The internal structure of lava flows- insights from AMS measurements I: Near vent a'a, J. Volcanol. Geotherm. Res. 70 (1996) 21–36.
[32] M.D. Knight, G.P.L. Walker, Magma flow directions in dikes of Koolau Complex, Oahu, determined from magnetic fabric studies, J. Geophys. Res. 93 (B5) (1988) 4301–4319.
[33] E. Canon-Tapia, H. Pinkerton, The anisotropy and magnetic susceptibility of lava flows: an experimental approach, J. Volcanol. Geotherm. Res. 98 (2000) 219–233.
[34] O. Merle, Numerical modelling of strain in lava tubes, Bull. Volcanol. 62 (2000) 53–58.